# Linear response range characterization and *in vivo* application of laser speckle imaging of blood flow dynamics

**Bernard Choi**
University of California, Irvine
Beckman Laser Institute and Medical Clinic
1002 Health Sciences Road East
Irvine, California 92612

**Julio C. Ramirez-San-Juan**
University of California, Irvine
Beckman Laser Institute and Medical Clinic
1002 Health Sciences Road East
Irvine, California 92612
and
Instituto Nacional de Astrofisica,
Optica y Electronica
Puebla, Mexico

**Justin Lotfi**
University of California, Irvine
Beckman Laser Institute and Medical Clinic
and School of Biological Sciences
1002 Health Sciences Road East
Irvine, California 92612

**J. Stuart Nelson**
University of California, Irvine
Beckman Laser Institute and Medical Clinic
1002 Health Sciences Road East
Irvine, California 92612

**Abstract.** Noninvasive blood flow imaging can provide critical information on the state of biological tissue and the efficacy of approaches to treat disease. With laser speckle imaging (LSI), relative changes in blood flow are typically reported, with the assumption that the measured values are on a linear scale. A linear relationship between the measured and actual flow rate values has been suggested. The actual flow rate range, over which this linear relationship is valid, is unknown. Herein we report the linear response range and velocity dynamic range (VDR) of our LSI instrument at two relevant camera integration times. For integration times of 1 and 10 ms, the best case VDR was 80 and 60 dB, respectively, and the worst case VDR was 20 and 50 dB. The best case VDR values were similar to those reported in the literature for optical Doppler tomography. We also demonstrate the potential of LSI for monitoring blood flow dynamics in the rodent dorsal skinfold chamber model. These findings imply that LSI can provide accurate wide-field maps of microvascular blood flow rate dynamics and highlight heterogeneities in flow response to the application of exogenous agents.  [DOI: 10.1117/1.2341196]

Keywords: laser Doppler flowmetry; window chamber; microvasculature; Doppler optical coherence tomography.

Paper 05276SSR received Sep. 27, 2005; revised manuscript received Feb. 27, 2006; accepted for publication Apr. 5, 2006; published online Aug. 31, 2006. This paper is a revision of a paper presented at the SPIE conference on Photonic Therapeutics and Diagnostics, Jan. 2005, San Jose, California. The paper presented there appears (unrefereed) in SPIE proceedings Vol. 5686.

## 1 Introduction

Noninvasive blood flow imaging can provide critical information on the state of biological tissue and the efficacy of approaches to treat disease. Fluorescein angiography is used routinely to study blood flow dynamics in the retina.[1] Laser Doppler flowmetry and laser Doppler imaging have been applied in numerous preclinical and clinical studies on the brain,[2,3] retina,[4,5] skin,[6,7] and joints.[8] Principles of Doppler shift imaging have been combined with optical coherence tomography to provide high-resolution cross-sectional images of blood flow.[9–17]

In 1981, Fercher and Briers[18] proposed a laser speckle imaging (LSI) approach as an alternative to laser Doppler imaging. On the basis of this study, it was concluded that variations in speckle contrast can be used to provide directly a wide-field velocity distribution map. LSI has since been employed for wide-field blood flow imaging of the brain,[2,19–22] retina,[18,23] and skin,[6,24–26] with high temporal resolution. Briers[27] has demonstrated that LSI and laser Doppler imaging provide equivalent assessments of blood flow.

With LSI, relative changes in blood flow are typically reported, with the assumption that the measured values are on a linear scale. A linear relationship between the measured and actual flow rate values has been suggested.[2,19] The actual flow rate range over which this linear relationship is valid is unknown. Knowledge of the relationship between measured and actual blood flow values is important because researchers would then know to which *in vitro* and *in vivo* flow models LSI could be applied to quantify relative flow changes.

The primary objective of this paper is to provide insight into the relationship between LSI measurements of speckle flow index with actual flow rate. The secondary objective is to demonstrate application of LSI to an *in vivo* rodent dorsal skinfold model and to show its potential as a wide-field microvascular imaging modality in a widely used animal model. Based on the analysis of Yuan et al.,[21] the central hypothesis was that image integration time would affect the overall velocity dynamic range and signal-to-noise ratio of LSI.

Address all correspondence to Bernard Choi, University of California, Irvine, Beckman Laser Institute, 1002 Health Science Rd. E, Irvine, CA 92612; Tel: 1 949 829-9491; Fax: 1 949 824-6969; E-mail: choib@uci.edu

1083-3668/2006/11(4)/041129/7/$22.00 © 2006 SPIE

## 2 Materials and Methods

### 2.1 *Relationship Between Speckle Flow Index and Actual Flow Rate*

The objective of this study was to establish the actual flow rate range over which a linear relationship existed with measured speckle flow index (SFI). To accomplish this objective, we developed a simple *in vitro* flow phantom to simulate blood flow in the rodent dorsal skinfold model. In the accompanying experiments, we varied flow rate and camera integration time.

#### 2.1.1 *Experimental Design*

*LSI instrument.* The instrument consists of a 30-mW, 633-nm helium-neon laser (Edmund Industrial Optics, Barrington, New Jersey), plano-convex lens, beam steering mirrors, digital charge-coupled device (CCD) camera (Retiga EXi, QImaging, Burnaby, British Columbia, Canada) equipped with a macro lens, and desktop Personal Computer (PC). Collimated light emitted from the laser became divergent after passing through the lens. To make the instrument more compact, mirrors were used to steer the diverging beam to the target plane. The resultant speckle pattern was imaged on the CCD array at 1:1 magnification and acquired to the PC memory. The *f*-stop of the macro lens was set to ensure a speckle size equivalent to the pixel dimensions ($6.45 \times 6.45\ \mu m^2$) of the camera.

*In vitro flow phantom.* To generate scattering agar gels, we heated a solution consisting of 100 mL of deionized water and 10 mL of glycerol to boiling. Glycerol was used to improve the mechanical integrity of the resultant gels. We added simultaneously 0.3 g of $TiO_2$ (Sigma, St. Louis, Missouri) and 2 g of agar to the heated solution. The former was used to increase the scattering coefficient of the otherwise clear gels, and the agar added was deemed appropriate to simulate the reduced scattering coefficient of skin, based on previous frequency domain photon migration experiments.[28] The solution was then poured into various molds (e.g., Petri dishes, sandwiched glass slides) to achieve the desired thickness (150 $\mu$m to several millimeters) and allowed sufficient time to solidify. In specific gels, an ~550-$\mu$m inner diameter glass capillary tube (Chase Instruments Corp., Glen Falls, New York) was embedded into the mold prior to solidification. A syringe-based infusion pump (Harvard Apparatus, Holliston, Massachusetts) was used to inject fluid into the flow tube. Tygon tubing delivered the fluid from the filled syringe mounted on the pump to the tube embedded in the gel. Five hundred mL of indated whole blood was obtained from the San Diego Blood Bank (San Diego, California) and used in this study.

*Experiments.* The infusion pump was set to achieve flow rates up to 21 mm/s. The flow phantom tube was imaged with the LSI instrument. Camera integration times of 1 and 10 ms were selected as representative values based on those used in previous studies.[2,6,19–22,25,26]

*LSI image analysis.* The image processing algorithm has been described previously in detail.[2,24] Briefly, the recorded image sequence was converted to speckle contrast images by applying a $7 \times 7$ sliding window to each $1392 \times 1040$ image. Although the $7 \times 7$ sliding window reduces the spatial resolution of our system, such a technique is necessary to preserve the assumption of first order speckle statistics.[27] Because the resultant speckle contrast image is essentially oversampled, relatively high spatial frequency details remain preserved in the speckle contrast and subsequent flow images. At each window position, the mean graylevel intensity ($\langle I \rangle$) and standard deviation ($\sigma$) were determined, and the speckle contrast ($K$) of the center pixel in the window can be computed as

$$K = \frac{\sigma}{\langle I \rangle}. \tag{1}$$

Assuming a Lorentzian flow velocity distribution,[29] the correlation time ($\tau_c$) of the intensity fluctuations can be calculated from:

$$K = \sqrt{\left\{ \frac{\tau_c}{2T}[1 - \exp(-2T/\tau_c)] \right\}}, \tag{2}$$

where $T$ is the camera integration time. Maple™ software (Maplesoft, Ontario, Canada) was used to obtain an analytic series expansion for $\tau_c$ as a function of $K$, for the values of $T$ used in this study. Relative flow images were obtained by calculating $1/\tau_c$ at each image pixel; a higher pixel value was assumed to be analogous to higher blood flow.

Because we were not concerned with real-time speckle flow imaging in this study, we performed the image processing offline. We selected a central $\sim 260 \times 260\ \mu m^2$ (i.e., $40 \times 40$ pixels) region of interest and computed the mean SFI. We then determined the mean SFI from images acquired at an actual flow rate of zero, corresponding to a background contribution from Brownian motion of scatterers. For further analysis, we used the difference between mean SFI values at nonzero actual flow rates and the background values.

### 2.2 *In Vivo Application of LSI*

The objective of this study was to demonstrate *in vivo* application of LSI. To accomplish this objective, we applied chemical agents to the microvascular network of the rodent dorsal skinfold chamber model.[25,30–37]

#### 2.2.1 *Experimental Design*

*Rodent dorsal skinfold chamber model.* Surgical installation of a dorsal skinfold window permitted observation of full-thickness skin from both the epidermal and subdermal sides (Fig. 1). The animal was anesthetized with a combination of Ketamine and Xylazine (4:3 ratio, 0.1 g/100 g body weight) administered by intraperitoneal injection. A section for window placement on the back of the animal was selected, surgically scrubbed, shaved, and depilated. Sutures attached to a temporary mount retracted the dorsal skin away from the animal's body. A circular section with an approximate diameter of 1 cm was cut from one side of the symmetrical skinfold, thus exposing blood vessels in the underlying skin. An aluminum chamber was sutured to both sides of the skin and the sutures cut to release the skin from the mount. To prevent dehydration, saline was applied periodically to the subdermal skin. The surgery was performed as defined in a protocol ap-

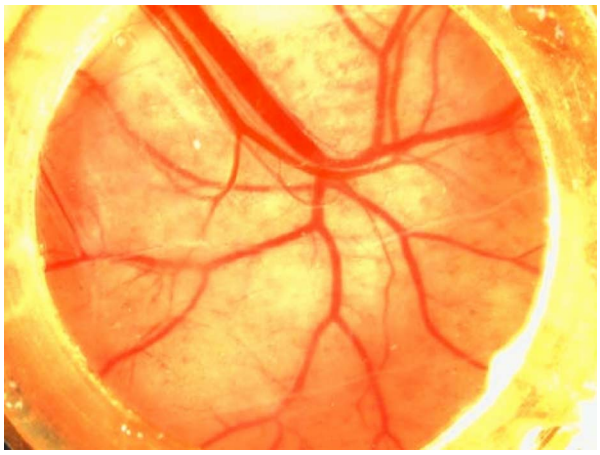

**Fig. 1** Representative subdermal image of a dorsal skinfold window chamber preparation.

proved by the University of California, Irvine, Animal Use Committee.

*Chemical agents.* We were interested in studying microvascular flow during the application of a recently developed polyurethane agent designed to reduce temporarily optical scattering in biological tissues such as skin.[38] The agent was applied directly to the subdermal microvascular network and LSI images acquired over a 15-min period from the subdermal side. Due to lateral diffusion of the agent away from the imaged microvascular network after application, the agent was reapplied on a regular basis during the image acquistion period. In separate experiments, each on a different animal, phosphate buffered saline and 13.6 M glycerol were applied as negative and positive controls, respectively, for inducing microvascular flow changes.

*Image acquisition and processing.* Raw speckle images were acquired and SFI images computed as described above. White light reflectance images were also acquired to serve as anatomical reference images. To visualize changes in blood flow induced by agent application, the SFI images were converted to binary images using the iterative selection method.[39] This automated method was used to determine a threshold SFI value based on an initial estimate $SFI_0$. The mean SFI values of all pixels below ($SFI_{below}$) and above ($SFI_{above}$) $SFI_0$ were calculated and a new estimate $SFI_{new}$ computed as the arithmetic mean of $SFI_{below}$ and $SFI_{above}$. This process was repeated with each new estimate until $SFI_{below}$ was equal to $SFI_{above}$.

With each experiment, a threshold SFI value was determined for the SFI image acquired immediately after agent application and was applied to binarize SFI images acquired at later time points. To visualize better arteriolar and venular blood flow dynamics, the binary SFI images were superimposed on the corresponding white light anatomical images.

## 3 Results

*Camera integration time impacts the relationship between measured SFIs and actual flow rate* (*Fig. 2*). With an increase in integration time from 1 to 10 ms, the following trends were observed with the *in vitro* flow phantom: (1) the linear response range decreased from 2 to 20 mm/s, to 0 to 5 mm/s; (2) the best case velocity resolution, defined as the reciprocal of the slope of a linear fit to the data, decreased from 2 to 5 $\mu$m/s; and (3) as shown by the correlation coefficient of the linear fits, the amount of scatter in the data decreased. Collectively, these data provide us with knowledge on the actual flow rate range over which our LSI instrument has a linear response.

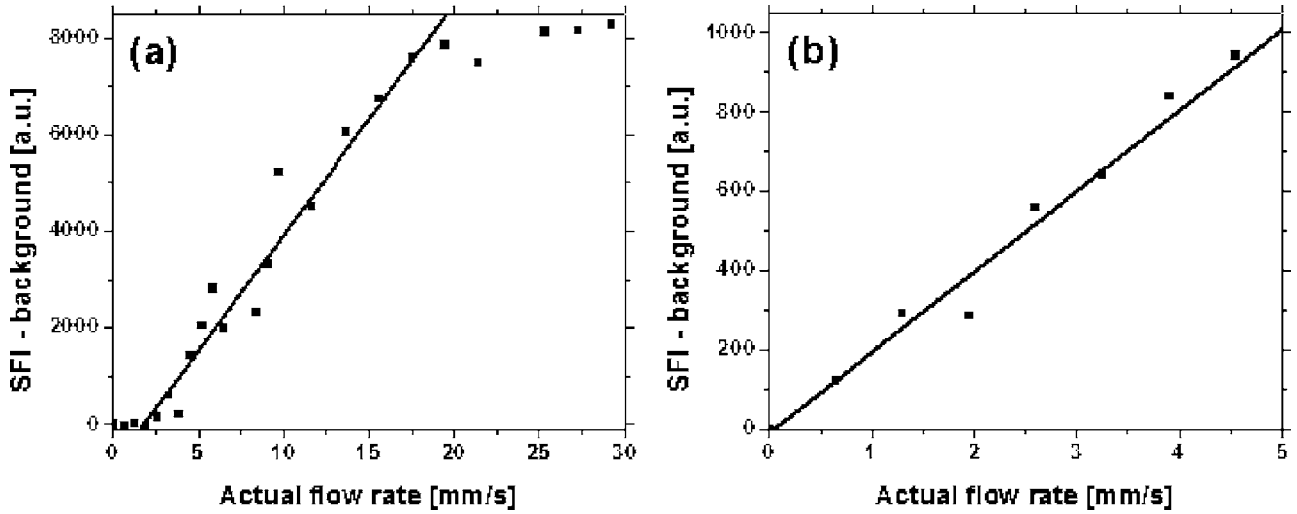


**Fig. 2** Effect of camera integration time on the linear response range between SFI and actual flow rate. Data acquired with integration times of (a) 1 and (b) 10 ms are presented. The data show that an increase in integration time decreases the linear response velocity range and velocity resolution and increases the linear regression fit to the discrete data points. In (a), the full set of acquired data is shown, and the linear fit is restricted to actual flow rate values of 2 to 20 mm/s.

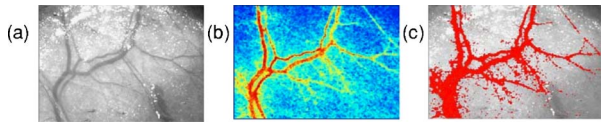


**Fig. 3** Representative (a) white light reflectance, (b) SFI, and (c) superimposed white light–binary SFI images of the microvascular network in the rodent dorsal skinfold chamber. Image dimensions are 9 $\times$ 6.8 mm$^2$.

*Wide-field, arteriolar, and venular blood flow dynamics are readily monitored during exogenous chemical agent application.* Representative white light, SFI, and superimposed white light–binary SFI images of the rodent dorsal skinfold window chamber are shown in Fig. 3. A good correspondence between visible blood vessels is evident from a comparison of the white light and SFI images and in the superimposed image. By applying the same threshold SFI value to all images acquired in a time-resolved sequence, blood flow dynamics are readily visualized in a qualitative fashion. With direct application of saline (i.e., negative control) to the microvascular network for 16 min, a slight increase in blood flow was observed, primarily in the smaller arteriolar and venular branches (Fig. 4). With direct application of glycerol (i.e., positive control) to the microvascular network, a gradual decrease in blood flow was observed (Fig. 5). From the superimposed white light–binary SFI image, we observed an immediate decrease in venular flow and a delayed decrease in arteriolar flow (between 12 and 16 min after glycerol application). With direct application of the polyurethane agent to the microvascular network, a slight increase in blood flow was observed in the smaller vessel branches (Fig. 6), similar to that observed with saline application. Collectively, these data demonstrate the potential of LSI to allow wide-field monitoring of heterogeneous blood flow dynamics.

## 4 Discussion

We are primarily interested in studying hemodynamics in *in vivo* microvascular network animal models, such as the dorsal skinfold window chamber preparation. Before we could use LSI reliably as a quantitative tool to assess blood flow in these models, we first needed to study the relationship between SFI and actual flow rate. In this study, we identified a range over which the relationship is linear, for two commonly used camera integration times. Specifically, we have shown that, for integration times of 1 and 10 ms, the linear relationship holds for flow rates of 2 to 20 and 0 to 5 mm/s, respectively (Fig. 2). There is slightly more scatter in the 1-ms integration time data than that at 10 ms and hence more deviation from the linear regression fit. A similar trend in improved speckle contrast-to-noise ratio was observed by Yuan et al.[21]

Our data suggest that camera integration time should be selected with the anticipated velocity range to be evaluated. Vargas et al.[15] used optical Doppler tomography to measure blood flow velocities of ~4 mm/s in arterioles and venules in the rodent dorsal skinfold model. From blood flow rates measured in arterioles and venules of the rodent cranial window model, velocities of less than 5 mm/s were anticipated.[32] To ensure that a linear relationship is maintained between measured speckle flow index values and actual flow rate, our data suggest an integration time of approximately 10 ms should be used to monitor flow rate dynamics directly in arterioles and venules. From the analysis of Yuan et al.,[21] the speckle contrast to noise ratio is only ~8% less at an integration time of 10 ms than the maximum ratio at 5 ms, which we believe is an acceptable compromise to ensure measurements are acquired over a linear response range.

The data obtained in this study can be used to estimate a velocity dynamic range (VDR) for our LSI instrument[10]

$$VDR = 20 \log\left(\frac{V_z}{\Delta V_z}\right), \tag{3}$$

where VDR is in units of decibels, $V_z$ is the velocity range, and $\Delta V_z$ is the velocity resolution. It is instructive to study two VDR limits, focusing on the linear response velocity range only: best case [i.e., $\Delta V_z$ equals the inverse of the slope of the regression line between SFI and actual flow rate (Fig. 2)]; and worst case (i.e., $\Delta V_z$ equals the quotient of the largest deviation from the regression line and the slope of the line). For integration times of 1 and 10 ms, the best case VDR is 80 and 60 dB, respectively, and the worst case VDR is 20 and 50 dB. The best case VDR values are similar to those reported by Yang et al.[10] for their optical Doppler tomography system. Thus, for blood flow characterization in superficial vessels such as those found in the rodent dorsal skinfold chamber, chick chorioallantoic membrane, and rodent cranial window, the performance of LSI is on par with optical coherence tomography.

We performed a series of experiments (Figs. 4 to 6) to demonstrate the potential of LSI for wide-field monitoring of blood flow dynamics in an *in vivo* microvascular network model. We observed a heterogeneous decrease in blood flow after glycerol application (Fig. 5), with an initial decrease in venules and a delayed decrease in arterioles. A similar trend

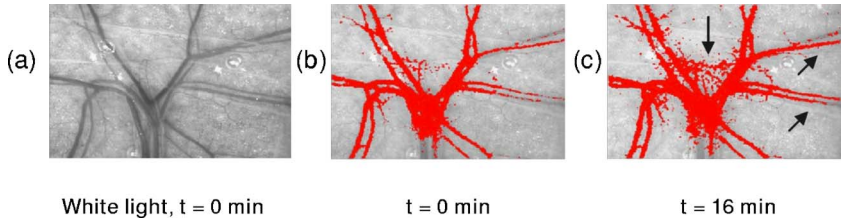


**Fig. 4** Representative (a) white light reflectance and (b, c) superimposed white light–binary SFI images at 0 and 16 min, respectively, after direct saline application to the microvascular network of the rodent dorsal skinfold chamber. The images show a slight increase in blood flow in the smaller blood vessel branches [(arrows in (c)]. Image dimensions are 9 $\times$ 6.8 mm$^2$.

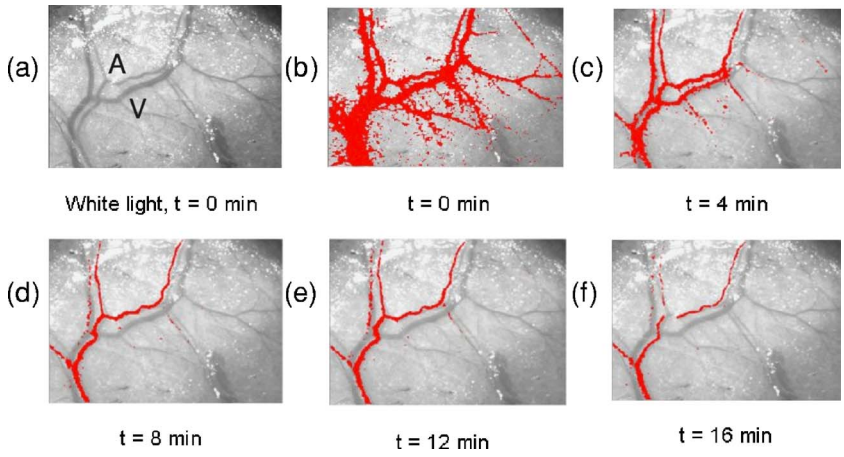


**Fig. 5** Representative (a) white light reflectance and (b to f) superimposed white light–binary SFI images at various time points after direct glycerol application to the microvascular network of the rodent dorsal skinfold chamber. The images show a heterogeneous decrease in blood flow, with an initial decrease in venular flow ["V" in (a)] and a delayed decrease in arteriolar flow ["A" in (a)]. Image dimensions are $9 \times 6.8$ mm$^2$.

was observed by Vargas et al.[15] with optical Doppler tomography monitoring of a single arteriole-venule pair. A potential advantage of LSI over such a technique is the ability to interrogate multiple vessels and associated branches simultaneously.

A surprising finding was that the blood flow rate increased slightly with application of phosphate buffered saline (Fig. 4) and the polyurethane agent (Fig. 6). The thermoregulatory aspect of cutaneous blood flow may have led to this increase, because the agent temperature (~25°C) was slightly lower than the *in vivo* skinfold temperature (~28°C). Another possibility is that the reduced access of the subdermal tissue to ambient oxygen due to the addition of saline may have led to a compensatory increase in blood flow to reestablish steady-state oxygenation conditions. The strong flow reduction effect of glycerol was probably sufficient to overcome any compensatory increase in blood flow due to either effect.

Our current LSI instrument is capable of raw speckle image acquisition rates of ~100 frames per s, which corresponds to a temporal resolution of ~10 ms. The intent of the current *in vivo* imaging study was to compare our data (Figs. 4 to 6) with previously published data,[15] so we acquired image sequences during agent application at a considerably slower frame rate of 0.5 frames per min. Previously, we have acquired raw speckle images within seconds after pulsed dye laser irradiation of select blood vessels,[25] demonstrating the potential of LSI to study rapid transients in blood flow.

With our optical imaging configuration, we acquired images at unity magnification to provide a raw speckle image lateral resolution of 6.45 $\mu$m. To achieve this spatial resolution, we selected the $f$-number of the macro lens so that the speckle size was equivalent to that of a single pixel[2]

$$w = 1.2(M+1)\lambda(f/\#), \tag{4}$$

where $w$ is the speckle size, $M$ is the optical magnification, and $f/\#$ is the $f$-number. Although the intent of the current study was to perform wide-field blood flow imaging of the dorsal skinfold window chamber preparation, it is possible to increase the optical magnification by selecting the appropriate zoom lens with a decreased $f/\#$ setting. The current hypothesis is that the speckle size should be equal to the size of a single pixel to achieve appropriate sampling of the speckle pattern.[24] Equation (4) sets an upper limit on the image mag-

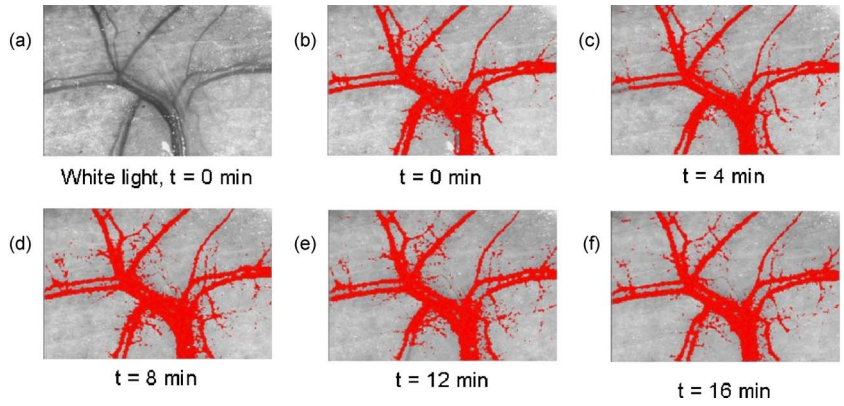


**Fig. 6** Representative (a) white light reflectance and (b to f) superimposed white light–binary SFI images at various time points after direct polyurethane application to the microvascular network of the rodent dorsal skinfold chamber. The images show a slight increase in blood flow in the smaller blood vessel branches. Image dimensions are $9 \times 6.8$ mm$^2$.

nification due primarily to the available $f/\#$ settings on commercially available lenses. To the best of our knowledge, a quantitative theoretical description to support the current hypothesis has not been proposed, so it may be possible to perform high-magnification LSI (i.e., "laser speckle microscopy") with an optical configuration that violates Eq. (4) We have planed a set of experiments to test the current hypothesis and will report our findings in a future publication.

Theoretical[27] and experimental[2] studies have established that LSI and laser Doppler imaging provide equivalent relative flow values. Thus, if the same laser wavelength is used, both methods interrogate perfusion within equivalent volumes of tissue. The primary advantages of LSI include its relative simplicity (i.e., no need for scanning mechanical components) and its image acquisition rate. LSI images can be acquired at the maximum camera frame rate (typically 30+ frames per s for 300+ kilopixel images) and processed offline. With laser Doppler imaging, acquisition times of several minutes are required to achieve a 65-kilopixel image.[6] Such prolonged acquisition times are associated with a considerably higher risk of motion artifact. Laser Doppler imaging does provide information on the direction of blood flow, a capability that is not present with conventional LSI. These considerations should be taken into account during selection of the appropriate wide-field blood flow imaging method.

The LSI velocity dynamic range and signal-to-noise ratio reported here provide an imaging platform that can be used to study normal and tumor microvasculature in the rodent dorsal skinfold model. Angiogenesis associated with tumor growth has been studied extensively with this animal model.[31,32,37] In such studies, blood flow dynamics are typically monitored with point laser Doppler probes or direct red blood cell counting algorithms. Coupling of LSI with other optical imaging modalities, such as reflectance,[22] fluorescence, and multiphoton microscopy, may enhance knowledge of critical factors such as heterogeneities in tumor blood flow and local oxygen consumption dynamics.

In summary, we have shown that SFI and actual flow rate have a linear relationship at typically used LSI integration times and at blood flow rate values typical of arterioles, venules, and capillaries. With an increase in integration time, the VDR decreases and signal-to-noise ratio increases. These findings imply that LSI can provide accurate wide-field maps of microvascular blood flow rate dynamics and highlight heterogeneities in flow response to the application of exogenous agents.

## Acknowledgments

The authors acknowledge financial support from the American Society for Laser Medicine and Surgery, Inc. (B.C.); the Arnold and Mabel Beckman Fellows Program (B.C.); the Beckman Foundation; the Fondo de Repatriaciones CONACYT-México (J.C.R.S.J.); and National Institutes of Health [Grants No. AR047551, EB02495, and AR048458, (J.S.N.); and the Laser Microbeam and Medical Program (LAMMP), a NIH Biomedical Technology Resource, Grant No. P41-RR01192, at the University of California, Irvine]. The authors thank Dr. Roger Chiu-Zarate (Beckman Laser Institute and Medical Clinic) for assistance with the LSI instrument software.

## References

1. Y. Tao, Y. R. Jiang, X. X. Li, C. Y. Yin, and M. Yao, "Fundus and histopathological study of radial optic neurotomy in the normal miniature pig eye,"*Arch. Ophthalmol. (Chicago)* **123**, 1097–1101 (2005).
2. A. K. Dunn, T. Bolay, M. A. Moskowitz, and D. A. Boas, "Dynamic imaging of cerebral blood flow using laser speckle," *J. Cereb. Blood Flow Metab.* **21**, 195–201 (2001).
3. S. A. Sheth, M. Nemoto, M. W. Guiou, M. A. Walker, and A. W. Toga, "Spatiotemporal evolution of functional hemodynamic changes and their relationship to neuronal activity," *J. Cereb. Blood Flow Metab.* **25**, 830–841 (2005).
4. R. D. Ferguson, D. X. Hammer, A. E. Elsner, R. H. Webb, and S. A. Burns, "Wide-field retinal hemodynamic imaging with the tracking scanning laser ophthalmoscope," *Opt. Express* **12**, 5198–5208 (2004).
5. C. E. Riva, E. Logean, and B. Falsini, "Visually evoked hemodynamical response and assessment of neurovascular coupling in the optic nerve and retina," *Prog. Retin Eye Res.* **24**, 183–215 (2005).
6. K. R. Forrester, J. Tulip, C. Leonard, C. Stewart, and R. C. Bray, "A laser speckle imaging technique for measuring tissue perfusion," *IEEE Trans. Biomed. Eng.* **51**, 2074–2084 (2004).
7. A. Boignard, M. Salvat-Melis, P. H. Carpentier, C. T. Minson, L. Grange, C. Duc, F. Sarrot-Reynauld, and J. L. Cracowski, "Local hyperhemia to heating is impaired in secondary Raynaud's phenomenon," *Arthritis Res. Ther.* **7**, R1103–R1112 (2005).
8. C. G. Egan, J. C. Lockhart, and W. R. Ferrell, "Pathophysiology of vascular dysfunction in a rat model of chronic joint inflammation," *J. Physiol. (London)* **557**, 635–643 (2004).
9. H. W. Ren, Z. H. Ding, Y. H. Zhao, J. J. Miao, J. S. Nelson, and Z. P. Chen, "Phase-resolved functional optical coherence tomography: simultaneous imaging of in situ tissue structure, blood flow velocity, standard deviation, birefringence, and Stokes vectors in human skin," *Opt. Lett.* **27**, 1702–1704 (2002).
10. V. X. D. Yang, M. L. Gordon, B. Qi, J. Pekar, S. Lo, E. Seng-Yue, A. Mok, B. C. Wilson, and I. A. Vitkin, "High speed, wide velocity dynamic range Doppler optical coherence tomography (Part I): System design, signal processing, and performance," *Opt. Express* **11**, 794–809 (2003).
11. B. J. Vakoc, S. H. Yun, J. F. de Boer, G. J. Tearney, and B. E. Bouma, "Phase-resolved optical frequency domain imaging," *Opt. Express* **13**, 5483–5493 (2005).
12. J. K. Barton and S. Stromski, "Flow measurement without phase information in optical coherence tomography images," *Opt. Express* **13**, 5234–5239 (2005).
13. V. X. D. Yang, Y. X. Mao, N. Munce, B. Standish, W. Kucharczyk, N. E. Marcon, B. C. Wilson, and I. A. Vitkin, "Interstitial Doppler optical coherence tomography," *Opt. Lett.* **30**, 1791–1793 (2005).
14. C. J. Pedersen, S. Yazdanfar, V. Westphal, and A. M. Rollins, "Phase-referenced Doppler optical coherence tomography in scattering media," *Opt. Lett.* **30**, 2125–2127 (2005).
15. G. Vargas, A. Readinger, S. S. Dozier, and A. J. Welch, "Morphological changes in blood vessels produced by hyperosmotic agents and measured by optical coherence tomography," *Photochem. Photobiol.* **77**, 541–549 (2003).
16. X. J. Wang, T. E. Milner, and J. S. Nelson, "Characterization of fluid flow velocity by optical Doppler tomography," *Opt. Lett.* **20**, 1337–1339 (1995).
17. Z. P. Chen, T. E. Milner, D. Dave, and J. S. Nelson, "Optical Doppler tomographic imaging of fluid flow velocity in highly scattering media," *Opt. Lett.* **22**, 64–66 (1997).
18. A. F. Fercher and J. D. Briers, "Flow Visualization by Means of Single-Exposure Speckle Photography," *Opt. Commun.* **37**, 326–330 (1981).
19. H. Y. Cheng, Q. M. Luo, S. Q. Zeng, S. B. Chen, J. Cen, and H. Gong, "Modified laser speckle imaging method with improved spatial resolution," *J. Biomed. Opt.* **8**, 559–564 (2003).
20. H. Y. Cheng, Q. M. Luo, S. Q. Zeng, S. B. Chen, W. H. Luo, and H. Gong, "Hyperosmotic chemical agent's effect on *in vivo* cerebral blood flow revealed by laser speckle," *Appl. Opt.* **43**, 5772–5777 (2004).
21. S. Yuan, A. Devor, D. A. Boas, and A. K. Dunn, "Determination of optimal exposure time for imaging of blood flow changes with laser speckle contrast imaging," *Appl. Opt.* **44**, 1823–1830 (2005).
22. A. K. Dunn, A. Devor, A. M. Dale, and D. A. Boas, "Spatial extent of oxygen metabolism and hemodynamic changes during functional

activation of the rat somatosensory cortex," *Neuroimage* **27**, 279–290 (2005).
23. M. Hirao, H. Oku, W. Goto, T. Sugiyama, T. Kobayashi, and T. Ikeda, "Effects of adenosine on optic nerve head circulation in rabbits," *Exp. Eye Res.* **79**, 729–735 (2004).
24. J. D. Briers, G. Richards, and X. W. He, "Capillary blood flow monitoring using laser speckle contrast analysis (LASCA)," *J. Biomed. Opt.* **4**, 164–175 (1999).
25. B. Choi, N. M. Kang, and J. S. Nelson, "Laser speckle imaging for monitoring blood flow dynamics in the *in vivo* rodent dorsal skinfold model," *Microvasc. Res.* **68**, 143–146 (2004).
26. T. K. Smith, B. Choi, J. C. Ramirez-San-Juan, J. S. Nelson, K. Osann, and K. M. Kelly, "Microvascular blood flow dynamics associated with photodynamic therapy and pulsed dye laser irradiation," *Lasers Surg. Med.* **38**, 532–539 (2006).
27. J. D. Briers, "Laser Doppler and time-varying speckle: A reconciliation," *J. Opt. Soc. Am. A Opt. Image Sci. Vis* **13**, 345–350 (1996).
28. S. MerriH (unpublished data).
29. J. W. Goodman, *Statistical Optics*, John Wiley & Sons, Inc., New York (1985).
30. J. K. Barton, A. J. Welch, and J. A. Izatt, "Investigating pulsed dye laser-blood vessel interaction with color Doppler optical coherence tomography," *Opt. Express* **3**, 251–256 (1998).
31. M. W. Dewhirst, S. Shan, Y. T. Cao, B. Moeller, F. Yuan, and C. Y. Li, "Intravital fluorescence facilitates measurement of multiple physiologic functions and gene expression in tumors of live animals," *Dis. Markers* **18**, 293–311 (2002).
32. R. K. Jain, L. L. Munn, and D. Fukumura, "Dissecting tumour pathophysiology using intravital microscopy," *Nat. Rev. Cancer* **2**, 266–276 (2002).
33. Q. Chen, S. Tong, M. W. Dewhirst, and F. Yuan, "Targeting tumor microvessels using doxorubicin encapsulated in a novel thermosensitive liposome," *Mol. Cancer Ther.* **3**, 1311–1317 (2004).
34. P. Cabrales, A. G. Tsai, and M. Intaglietta, "Alginate plasma expander maintains perfusion and plasma viscosity during extreme hemodilution," *Am. J. Physiol. Heart Circ. Physiol.* **288**, H1708–H1716 (2005).
35. N. Isaka, T. P. Padera, J. Hagendoorn, D. Fukumura, and R. K. Jain, "Peritumor lymphatics induced by vascular endothelial growth factor-C exhibit abnormal function," *Cancer Res.* **64**, 4400–4404 (2004).
36. P. Babilas, G. Shafirstein, W. Baumler, J. Baier, M. Landthaler, R. M. Szeimies, and C. Abels, "Selective photothermolysis of blood vessels following flashlamp-pumped pulsed dye laser irradiation: *In vivo* results and mathematical modelling are in agreement," *J. Invest. Dermatol.* **125**, 343–352 (2005).
37. B. S. Sorg, B. J. Moeller, O. Donovan, Y. Cao, and M. W. Dewhirst, "Hyperspectral imaging of hemoglobin saturation in tumor microvasculature and tumor hypoxia development," *J. Biomed. Opt.* **10**, 044004 (2005).
38. M. Khan, B. Choi, S. Chess, K. Kelly, J. McCullough, and J. S. Nelson, "Optical clearing of *in vivo* human skin: Implications for light-based diagnostic imaging and therapeutics," *Lasers Surg. Med.* **34**, 83–85 (2004).
39. T. W. Ridler and S. Calvard, "Picture thresholding using an iterative selection method," *IEEE Trans. Syst. Man Cybern.* **8**, 630–632 (1978).